



# Mn(II)–amino acid complexes intercalated in CaAl-layered double hydroxide – Well-characterized, highly efficient, recyclable oxidation catalysts



Gábor Varga<sup>a,b</sup>, Ákos Kukovecz<sup>c,d</sup>, Zoltán Kónya<sup>c,e</sup>, László Korecz<sup>f</sup>, Szabolcs Muráth<sup>a,b</sup>, Zita Csenedes<sup>a,b</sup>, Gábor Peintler<sup>b,g</sup>, Stefan Carlson<sup>h</sup>, Pál Sipos<sup>b,i</sup>, István Pálinkó<sup>a,b,\*</sup>

<sup>a</sup> Department of Organic Chemistry, University of Szeged, Dóm tér 8, Szeged H-6720, Hungary

<sup>b</sup> Materials and Solution Structure Research Group, Institute of Chemistry, University of Szeged, Aradi Vértanúk tere 1, Szeged H-6720, Hungary

<sup>c</sup> Department of Applied and Environmental Chemistry, University of Szeged, Rerrich Béla tér 1, Szeged H-6720, Hungary

<sup>d</sup> MTA-SZTE “Lendület” Porous Nanocomposites Research Group, Rerrich Béla tér 1, Szeged H-6720, Hungary

<sup>e</sup> MTA-SZTE Reaction Kinetics and Surface Chemistry Research Group, Rerrich Béla tér 1, Szeged H-6720, Hungary

<sup>f</sup> Research Center for Natural Sciences, Hungarian Academy of Sciences, P.O. Box 286, Budapest H-1519, Hungary

<sup>g</sup> Department of Physical Chemistry and Materials Science, University of Szeged, Aradi Vértanúk tere 1, Szeged H-6720, Hungary

<sup>h</sup> Max-IV Laboratory, Lund University, Lund, Sweden

<sup>i</sup> Department of Inorganic and Analytical Chemistry, University of Szeged, Dóm tér 7, Szeged H-6720, Hungary

## ARTICLE INFO

### Article history:

Received 13 November 2015

Revised 19 December 2015

Accepted 22 December 2015

### Keywords:

Mn(II)–amino acid complexes in CaAl-LDH

Methods of synthesis

Structural characterization

Catalytic properties in oxidation reactions

## ABSTRACT

Intercalated composite materials were prepared with CaAl-layered double hydroxide as the host and Mn(II)–amino acid (L-cysteine, L-histidine and L-tyrosine) complex anions as the guest. Two methods (intercalation of the ligand first followed by constructing the complex; preforming the complex first, then introducing it among the layers of the host) and optimization of the auxiliary conditions were performed to arrive at composites having the complex exclusively among the layers. The obtained substances were structurally characterized by powder X-ray diffractometry, mid IR spectroscopy in diffuse reflectance mode and with ATR or photoacoustic detections, and scanning electron microscopy. The structural features of the intercalant (coordination number, coordination sites) were elucidated by classical chemical and energy dispersive X-ray analyses, EPR, X-ray absorption and far IR spectroscopies. Structural models are also given. The catalytic activities, selectivities and recycling abilities of the substances were studied in the oxidation reactions of cyclohexene with peracetic acid and *in situ* formed iodossylbenzene as oxidants and allylic alcohol with peracetic acid, in the liquid phase. The intercalated substances proved to be efficient and highly selective (with peracetic acid: outstanding epoxide, with iodossylbenzene superior diol selectivities) catalysts with very good recycling abilities.

© 2016 Elsevier Inc. All rights reserved.

## 1. Introduction

There are many routine ways of preparing layered double hydroxides (LDHs) [1,2]. One of the most often used methods is the co-precipitation of two (or more) precursors with a base, for instance, and most often, with an aqueous solution of NaOH at constant pH. The resulting material has typical X-ray diffractogram [3]. For CaAl-LDH, the host material of this study, indexing is described in Ref. [4]. Although, in the followings, we are going to call this material pristine CaAl-LDH, it is an intercalated system having

simple charge-compensating anions and water molecules among the layers. The basal distance (the interlayer distance plus one layer) can be readily calculated by using the Bragg equation, from the position of the first reflection.

It is known that with more or less ease, the anions can be exchanged for other anions, even for voluminous organic or complex ones [5,6]. Many methods are known for this procedure [7] (direct anion exchange from water [8], aqueous ethanol or acetone [9]; co-precipitation of the components [10]; heat treatment of the host, then recrystallization in the presence of the guest – this is the dehydration-rehydration method of intercalation – [11,12], milling or simple grinding the constituents [13,14], etc.); nevertheless, it is by far not as trivial as the synthesis of the pristine LDH. Quite often, the method that is efficient for one bulkier anion, will

\* Corresponding author at: Department of Organic Chemistry, University of Szeged, Dóm tér 8, Szeged H-6720, Hungary. Fax: +36 62 544 200.

E-mail address: [palinko@chem.u-szeged.hu](mailto:palinko@chem.u-szeged.hu) (I. Pálinkó).

not work for the other, even if the structures of the anions to be intercalated are similar. Even though the experienced researcher may have some rules of thumb for which technique to use, mostly the trial and error method remains the viable possibility. The successful intercalation does not destroy the layered structure, only the interlayer distance grows. This can be easily detected by powder X-ray diffractometry. The shift in the position of the first reflection or the appearance of a reflection at angles lower than the first reflection of the pristine LDH is an obvious sign of full or partial intercalation, respectively. Therefore, it is not surprising that powder XRD is a major characterizing tool in LDH chemistry. Nevertheless, the intercalation can be successful, if there is no change in the position of the first reflection; it may only mean that there is a position for the intercalant among the layers, which does not require the expansion of the layers. One may immediately conclude that it is very useful, if other characterization tools, which can verify or disprove intercalation, are also at hand.

Keeping all these in mind, in this contribution, the reader is led through our experience in trying to construct Mn(II)–amino acid complexes among the layers of CaAl-LDH. It is also intended to show through the oxidative transformations of cyclohexene and allylic alcohol that these materials are highly efficient and recyclable catalysts, and with the properly chosen oxidants, even the selectivity of the catalyzed reactions can be changed significantly.

Metal complexes have already been incorporated in LDHs, and the early works have been reviewed [15]. However, the Mn(II) complexes were scarcely involved either in the early contributions [15] or more recently [16–22]. Various prochiral olefins were epoxidized by oxygen or air over Mn(III)–sulfonato–salen complex incorporated in ZnAl-LDH [16–21]. The Mn–salen complex sandwiched between the layers of MgAl-LDH proved to be a stable recyclable catalyst in the N-oxidation of picoline [22]. A Mn–porphyrin derivative complex intercalated in a hydrophobically modified ZnAl-LDH was used for the epoxidation of various alkenes (cyclohexene, heptylene, phenylethylene, 3-methyl-3-buten-1-ol, ethyl cinnamate and chalcone) with oxygen [23].

However, the ligands have never been amino acids nor the host was CaAl-LDH in any of these works, and in this contribution, a more comprehensive characterization of the intercalated system was performed than in these previous studies.

## 2. Experimental

### 2.1. Materials and the methods of syntheses

The pristine Ca<sub>2</sub>Al-LDH samples were prepared from the precursor salts by the co-precipitation method. A mixture of Ca(NO<sub>3</sub>)<sub>2</sub> × 4H<sub>2</sub>O (30 mmol) and Al(NO<sub>3</sub>)<sub>3</sub> × 9H<sub>2</sub>O (15 mmol) was dissolved in 100 ml of distilled water and was stirred at pH 13 (set by 3 M NaOH) for 12 h. The suspension was filtered and dried for 24 h.

The intercalation of the Mn–amino acid complexes was attempted by direct anion exchange, however, by two distinctly different methods. In *Method 1*, the amino acid anions were intercalated first, and it was followed by the introduction of the Mn<sup>2+</sup> anions. In the first step, 2.5 × 10<sup>−4</sup> mols of L-cysteine, L-histidine or L-tyrosine were used for the intercalation. The manganese ions were introduced in solution, in various amounts (the ratio of amino acid and manganese ions were varied from 1:2 to 1:6). In order to identify the optimum conditions, the solvents (aqueous ethanol, aqueous acetone or water) and the pH (from 7.5 to 9.5) were also varied. The designation of composites prepared with *Method 1* will be Ca<sub>2</sub>Al–Mn(II)–amino acid anion–LDH. In *Method 2*, the Mn–amino acid complexes were prepared separately applying the same amounts and ratios, and varying the solution and the pH in the same way as in *Method 1*. Then, the solution containing the com-

plex was used for the intercalation. The designation of the composites prepared with *Method 2* will be Mn(II)–amino acid anion–Ca<sub>2</sub>Al-LDH.

All synthetic operations were performed under N<sub>2</sub> protecting gas to exclude airborne CO<sub>2</sub>, reacting with the water content of the LDH forming carbonate ion, which readily intercalates, blocking the introduction of any other anion.

All the applied compounds were the products of analytical grade from Sigma–Aldrich, and they were used as received.

### 2.2. Methods of characterization

Powder X-ray patterns were recorded by a Rigaku XRD-6000 diffractometer, using Cu K $\alpha$  radiation ( $\lambda$  = 0.15418 nm) at 40 kV, 30 mA. The UV/Vis spectroscopy was used for the quantitative analysis of amino acids at the wavelengths specific for the amino acid measured (L-cysteine: 231 nm, L-histidine: 210.5 nm and L-tyrosine: 273.5 nm). The members of the calibration series as well as the unknown samples were measured on a Shimadzu UV-1650 spectrophotometer. The morphologies of the samples were investigated with a scanning electron microscope (SEM, Hitachi S-4700, accelerating voltages of 10–18 kV). Energy-dispersive X-ray (EDX) data were obtained with a Röntec QX2 energy dispersive microanalytical system from two different parts of the sample. The coupled system (SEM-EDX) also provided with the elemental map.

The amount of metal ions between the layers was measured by a Thermo's IRIS Intrepid II ICP-OES spectrometer. Before measurements, a few milligrams of the intercalated complexes measured by analytical accuracy were digested in 1 cm<sup>3</sup> of cc. H<sub>2</sub>SO<sub>4</sub>; then, they were diluted with distilled water to 50 cm<sup>3</sup> and filtered.

The XAS measurements were carried out on the K edge of the manganese at MAX-lab, at beamline I811. This is a superconducting multipole wiggler beamline equipped with a water-cooled channel cut Si(111) double crystal monochromator delivering at 10 keV, approximately 2 × 10<sup>15</sup> photons/s/0.1% bandwidth with horizontal and vertical FWHM of 7 and 0.3 mrad, respectively. A beam-size of 0.5 mm × 1.0 mm (width × height) was used. The incident beam intensity (I<sub>0</sub>) was measured with an ionization chamber filled with a mixture of He/N<sub>2</sub>. Higher order harmonics were reduced by detuning the second monochromator to 70% of the maximum intensity. Data collection was performed in fluorescent mode. The samples were contained in Teflon spacers with Kapton tape windows according to the manganese concentration. The data were treated with the EXAFSPAK package [24].

The combination of three different IR techniques was applied for determining the positions of the amino acid anions and/or the anionic forms of the complexes. The instrument for recording the spectra was a BIO-RAD Digilab Division FTS-65A/896 FT-IR spectrophotometer with 4 cm<sup>−1</sup> resolution. The 4000–600 cm<sup>−1</sup> wavenumber range was recorded, but the most relevant 1850–600 cm<sup>−1</sup> range is displayed and discussed. 256 scans were collected for each spectrum. The spectra of each sample were taken in the diffuse reflectance mode (observing both the surface and the bulk of the samples) and using a MTEC 200 photoacoustic (PA) detector (scan speed of 2500 Hz – exploring the composition of the bulk) as well as a single reflection diamond ATR accessory (detecting organic material on the surface of the LDH).

For the identification of Mn–O(S and/or N) vibrations, the far IR spectra were recorded with a BIO-RAD Digilab Division FTS-40 vacuum FT-IR spectrophotometer (4 cm<sup>−1</sup> resolution, 256 scans). The Nujol mull technique was used between two polyethylene windows (the suspension of 10 mg sample and a drop of Nujol mull).

EPR spectroscopy was used for gathering information on the structure of the complexes. The spectra were recorded with a BRUKER EleXsys E500 spectrometer (microwave frequency 9.51 GHz,

microwave power 12 mW, modulation amplitude 5 G, modulation frequency 100 kHz) in quartz EPR tubes at room temperature. Approximately 10 mg of samples were used for each measurement, and their spectra were recorded without any additional sample preparation. All recorded EPR spectra were simulated by an EPR computer program [25].

### 2.3. Testing the catalytic activity

The catalytic activities of the intercalated substances were studied in the oxidative transformations of cyclohexene in the liquid phase. In order to find the optimal conditions, the reaction time (1–24 h), the amount of the catalyst (5–45 mg), the reaction temperature (15–55 °C), and the solvents (acetone, ethanol, dichloromethane) were altered. Furthermore, the oxidants (peracetic acid, (diacetoxy)iodobenzene) were also changed, to see whether it causes significant changes in reaction selectivities (distribution of the products in mol%). The optimum conditions were as follows: 25 mg of catalyst, 10 cm<sup>3</sup> of solvent (acetone when peracetic acid was used; aqueous acetone (5% water, 95% acetone by volume) when (diacetoxy)iodobenzene was applied), 5 mmol of cyclohexene, 2.5 mmol of oxidant, 3 h reaction time at 298 K.

Beside cyclohexene, the oxidative transformations of allylic alcohol were also investigated in the liquid phase using peracetic acid as the oxidant. Reaction parameters were optimized in a way similar to those used for the reactions using cyclohexene. The optimum reaction conditions were identified as follows: 60 mg of catalyst, 10 cm<sup>3</sup> of acetone as the solvent, 5 mmol of allylic alcohol, 2.5 mmol of peracetic acid, and 6 h reaction time at 333 K.

After 3 or 6 h of continuous stirring at the reaction temperature, the mixture was analyzed quantitatively by a Hewlett–Packard 5890 Series II gas chromatograph (GC) equipped with flame ionization detector, using an Agilent HP-1 column and the internal standard technique. The temperature was increased in stages from 50 °C to 250 °C. The products were identified *via* using authentic samples.

Conversion as well as turnover frequency (TOF) data are given. The former is defined as the percentage of the reactant consumed and the latter as the number of molecules reacted at one Mn(II) ion in 1 h.

## 3. Results and discussion

In the X-ray diffractograms, the appearance of the first reflection at lower angles than that for the pristine sample is a sign of successful intercalation. Nevertheless, it may occur that the reflections of the pristine sample also remain visible in the diffractogram. Then, the intercalation process did not go to completion. Even if the new reflections are only seen, *i.e.*, intercalation went to completion, it may happen that the intercalated anion is adsorbed on the outer surface as well, and certain amount stays there in spite of the intense washing with the solvent mixture used for intercalation. Finally, intercalation can be successful even if there is no change in the position of the first reflection. In this case, the anion to be intercalated is not so voluminous that would require enlarged interlayer space.

To be fully convinced that intercalation was indeed successful, and the intercalated moieties are among the layers exclusively, infrared spectroscopy can be utilized as a complementary technique.

In the experimental work leading to this contribution, diffuse reflectance spectroscopy was always applied because of the very easy sample preparation. However, it can only indicate the presence of the organic anion together with the LDH, but one cannot

give the position of the anion for sure, except in very fortunate cases, when large shifts in the vibrations of functional groups (mostly of carboxylate group) directly involved in the intercalation process can be identified. However, if one applies both a surface sensitive detection technique (ATR) and a bulk-sensitive one (PA) for the same sample, a comparison of the obtained spectra can convincingly reveal the location of the organic moiety.

### 3.1. Structural characterization by X-ray diffractometry and vibrational spectroscopy – selecting the intercalated samples

It was aimed to select the samples from those of the prepared, which had the complexes exclusively among the layers. Even though the samples having the complexes attached to the outer surface may also work as catalysts, these materials are less defined, and the loosely attached complexes are more prone to leaching during the reactions than those having them among the layers.

#### 3.1.1. Mn(II)-cysteinate-containing Ca<sub>2</sub>Al-LDH

The simplest cases to start with are the Mn-cysteinate-containing samples. The diffractograms in **SFigs. 1 and 2** (SFig. designates the figures included in the **Supplementary Material**) reveal that there is shift in the position of the first reflection only for Mn(II)-cysteinate–Ca<sub>2</sub>Al-LDH, *i.e.*, intercalation did occur. The intercalated cysteinate-containing complex could be prepared by *Method 2*. The diffractograms of the pristine and the intercalated Ca<sub>2</sub>Al-LDH are shown in **Fig. 1**. Here, the basal spacing (*d*) increased from 0.857 nm to 0.921 nm due to intercalation.

The composite material was analyzed for its Mn(II) and amino acid contents, and their ratios were calculated. Data listed in **Table 1** indicate that the nominal ratio was close to the experimentally obtained one.

The ATR-IR spectra of the pristine CaAl-LDH (**Fig. 2**, trace A) and Mn(II)-cysteinate–Ca<sub>2</sub>Al-LDH (**Fig. 2**, trace C) are very similar to each other indicating that practically no complex is bonded to the outer surface of the LDH. However, the PA-IR spectrum (**Fig. 2**, trace D) reveals that there was organic material intercalated among the LDH layers. The extra bands, which can only originate from the amino acid ligands, are at about the same wavenumber values as for the DRS-IR spectrum.

#### 3.1.2. Mn(II)-histidinate-containing Ca<sub>2</sub>Al-LDH

A comparison of **SFigs. 3 and 4** revealed two samples with successful intercalation. They are Ca<sub>2</sub>Al–Mn-histidinate–LDHs with

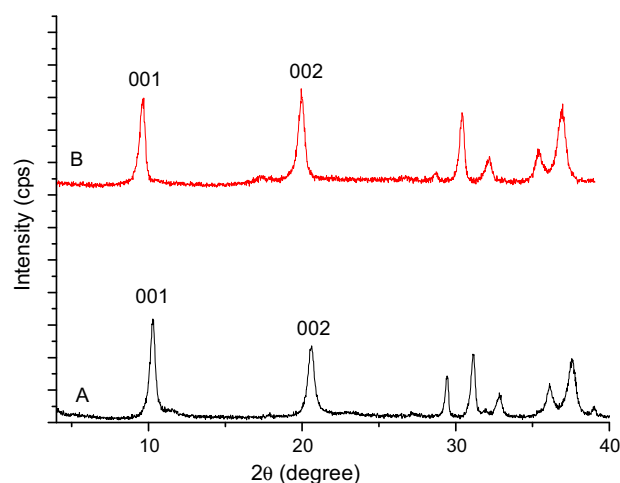


**Fig. 1.** X-ray diffractograms of: A: Ca<sub>2</sub>Al-LDH, B: Mn(II)-cysteinate–Ca<sub>2</sub>Al-LDH, aqueous ethanol, Mn:Cys = 1:2, pH = 8.5.

**Table 1**  
Quantitative analysis of the intercalant in the selected composite LDHs.

Composites	Amino acid (mol/0.3 g LDH)	Mn(II) (mol/0.3 g LDH)	Amino acid/Mn (II)
Mn(II)-cysteinate–Ca <sub>2</sub> Al-LDH, aqueous alcohol, pH = 8.5	$2.32 \times 10^{-4}$	$1.04 \times 10^{-4}$	2.23
Ca <sub>2</sub> Al–Mn(II)-histidinate–LDH, aqueous ethanol, pH = 8.5	$2.29 \times 10^{-4}$	$1.06 \times 10^{-4}$	2.16
Mn(II)-tyrosinate–Ca <sub>2</sub> Al-LDH, aqueous alcohol, pH = 7.5	$2.20 \times 10^{-4}$	$1.06 \times 10^{-4}$	2.08

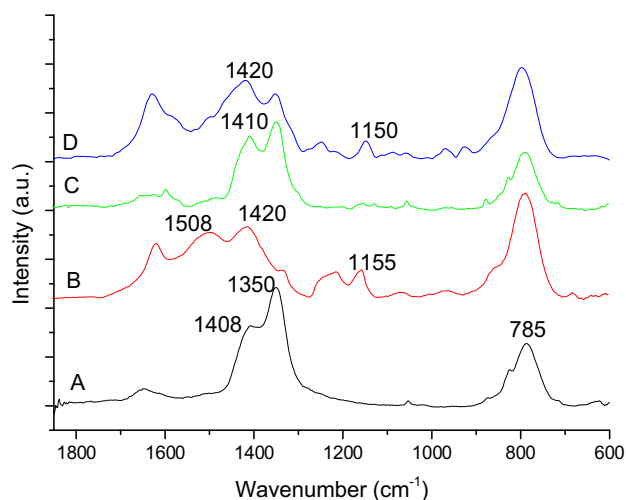


**Fig. 2.** Mid-range infrared spectra of: A: Ca<sub>2</sub>Al-LDH (ATR), B: Mn(II)-cysteinate–Ca<sub>2</sub>Al-LDH, (DRS), C: Mn(II)-cysteinate–Ca<sub>2</sub>Al-LDH, (ATR), D: Mn(II)-cysteinate–Ca<sub>2</sub>Al-LDH (PA); aqueous ethanol, pH = 8.5.

nominal Mn:His ratios of 1:2 and 1:4. This means that here, *Method 1* has worked successfully. However, the analysis of the IR spectra registered by ATR and PA detections (S*Figs. 5 and 6*) indicated that the sample with Mn:His ratio of 1:4 had amino acid anion over the outer surface too, as opposed to the one with the nominal Mn:His ratio of 1:2. This latter sample had the organic matter among the layers. Indeed, for this sample, an actual Mn:His ratio of close to 1:2 was obtained by the quantitative analysis of the metal cation and the amino acid anion (Table 1, row 3).

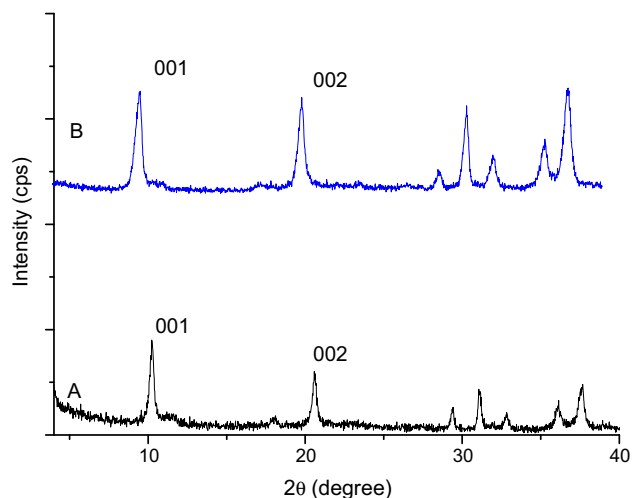


**Fig. 3.** X-ray diffractograms of: A: Ca<sub>2</sub>Al-LDH, B: Ca<sub>2</sub>Al–Mn(II)-histidinate–LDH; Mn:His = 1:2, pH = 8.5, aqueous ethanol.

The X-ray diffractogram and the IR spectra registered by various ways are seen in *Figs. 3 and 4*, respectively. Here, the *d* value increased from 0.857 nm to 0.929 nm due to intercalation.

Repeating the previously described reasoning, the ATR-IR spectra of the pristine CaAl-LDH (*Fig. 4*, trace A) and Ca<sub>2</sub>Al–Mn(II)-histidinate–LDH (*Fig. 4*, trace C) are very similar to each other, *i.e.*, organic material was not attached to the outer surface of the LDH. The PA-IR spectrum (*Fig. 4*, trace D) reveals that the histidinate ions were situated only among the LDH layers. The extra bands appeared approximately at the same wavenumber values as in the DRS-IR spectrum.

### 3.1.3. Mn(II)-tyrosinate-containing Ca<sub>2</sub>Al-LDH

Here, the situation was the most complicated. The solvent was water, in which the syntheses worked at all (S*Figs. 7 and 8*). However, there was no shift in the position of the first reflection. Applying *Method 2*, at very high (1:6) Mn:Tyr ratio, the LDH was of low quality, and the first reflection shifted toward higher degrees, indicating shrinkage instead of swelling (S*Fig. 7*). The infrared spectra taken by ATR and PA detectors (S*Figs. 9 and 10*) made it clear that intercalation did occur, and it was only “clean” (no organic matter on the outer surface) for the Mn(II)-tyrosinate–Ca<sub>2</sub>Al-LDH with Mn(II):Tyr ratio of 1:2, synthesized by *Method 2*.

The relevant X-ray diffractogram and the IR spectra registered by various ways are shown in *Figs. 5 and 6*, respectively. Here, the *d* value only increased slightly, from 0.857 nm to 0.859 nm during the intercalation. However, the ATR-IR spectra (*Figs. 6*, traces A and B) showed no organic matter on the outer surface, and the PA-IR spectrum (*Fig. 6*, trace D) verified its presence among the layers.

It is to be noted that the actual and nominal Mn:Tyr ratios were found to be close to each other (Table 1, last row).

The positions of the first (001) reflections of the pristine Ca<sub>2</sub>Al-LDH and the samples having the Mn(II)-amino acid complexes intercalated are summarized and the corresponding basal spacings are summarized in Table 2.

### 3.2. Morphologies of the intercalated samples

The selected intercalated substances displayed the laminar hexagonally shaped morphology, typical of LDHs (*Fig. 7*).

EDX measurement provided additional proof that sulfur-containing compounds were in the Mn(II)-cysteinate–Ca<sub>2</sub>Al-LDH

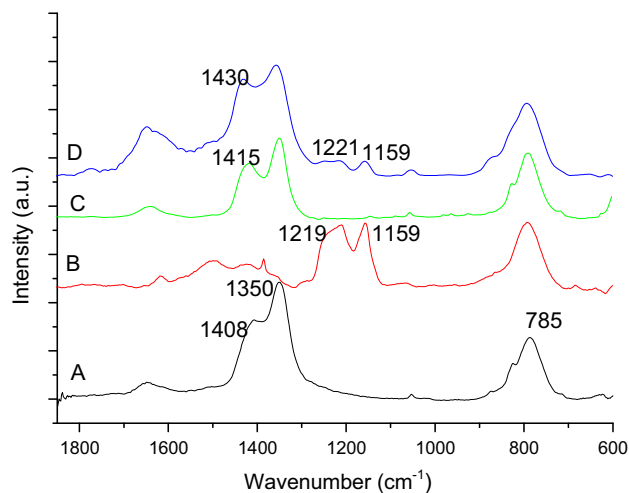


**Fig. 4.** Mid-range infrared spectra of: A: Ca<sub>2</sub>Al-LDH (ATR), B: Ca<sub>2</sub>Al–Mn(II)-histidinate–LDH (DRS), C: Ca<sub>2</sub>Al–Mn(II)-histidinate–LDH (ATR), D: Ca<sub>2</sub>Al–Mn(II)-histidinate–LDH (PA), for B–D, Mn:His = 1:2, aqueous ethanol, pH = 8.5.

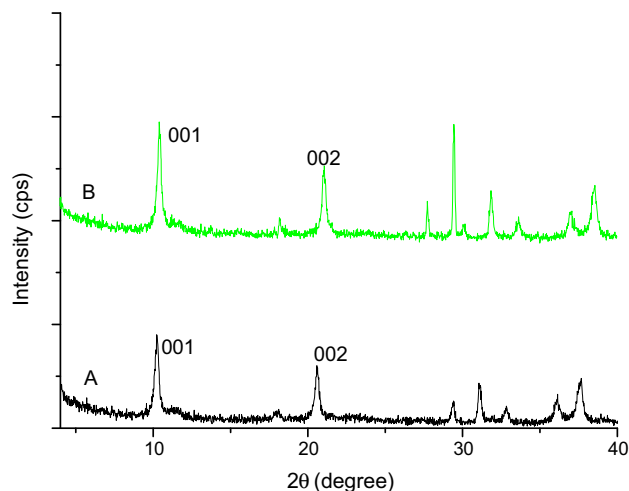


**Fig. 5.** X-ray diffractograms of: A:  $\text{Ca}_2\text{Al-LDH}$ , B:  $\text{Mn(II)-tyrosinate-Ca}_2\text{Al-LDH}$ ,  $\text{Mn:Tyr} = 1:2$ , water,  $\text{pH} = 8$ .

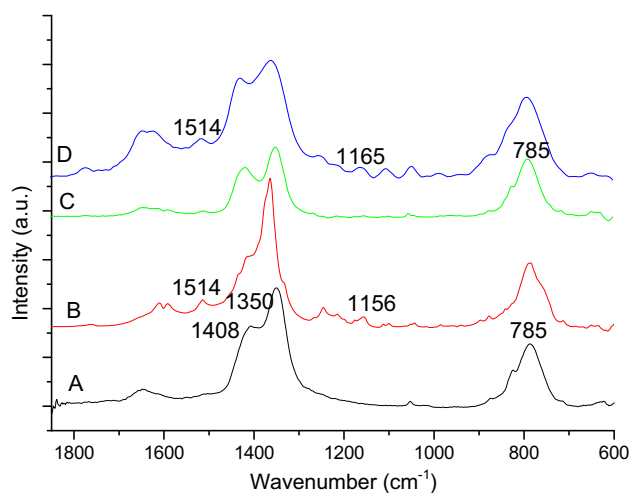


**Fig. 6.** Mid-range infrared spectra of: A:  $\text{Ca}_2\text{Al-LDH}$  (ATR), B:  $\text{Mn(II)-tyrosinate-Ca}_2\text{Al-LDH}$  (DRS), C:  $\text{Mn(II)-tyrosinate-Ca}_2\text{Al-LDH}$  (ATR), D:  $\text{Mn(II)-tyrosinate-Ca}_2\text{Al-LDH}$  (PA);  $\text{Mn:Tyr} = 1:2$ , water,  $\text{pH} = 8$ .

**Table 2**

The positions of the 001 reflections and the corresponding basal (*d*) spacings in the pristine LDH and the intercalated derivatives.

LDHs	001 reflection ( $^\circ$ )	<i>d</i> spacing (nm)
$\text{Ca}_2\text{Al-LDH}$	10.32	0.857
$\text{Mn(II)-tyrosinate-Ca}_2\text{Al-LDH}$	10.30	0.859
$\text{Mn(II)-cysteinate-Ca}_2\text{Al-LDH}$	9.60	0.921
$\text{Ca}_2\text{Al-Mn(II)-histidinate-LDH}$	9.52	0.929

composite (Fig. 8). In the previous measurements, it was shown that the complexes were only among the layers.

### 3.3. Characterization of the intercalant

The amino acid to  $\text{Mn(II)}$  ratios shown in Table 1 reveal that the amino acid anions may have behaved as multidentate ligands. In the  $\text{Ca}_2\text{Al-Mn(II)-histidinate-LDH}$  the carboxylic group as well as the imidazole ring must have been deprotonated.

$\text{Mn(II)}$  ions in the composite were also verified by EPR as well as XAS measurements. EPR spectra contain narrow lines on a broad

structureless background (from  $\text{Mn(II)}$  ions with dipolar interaction). The decomposed EPR spectra of the  $\text{Ca}_2\text{Al-Mn(II)-histidinate-LDH}$  and  $\text{Mn(II)-cysteinate-Ca}_2\text{Al-LDH}$  are shown in Fig. 9.

Both measured spectra show six well-resolved hyperfine lines, originating from the interaction of the electron spin with the nuclear spin ( $^{55}\text{Mn}$ ,  $I = 5/2$ ). Due to the significant zero-field interaction, the sextet lines of  $\text{Mn}^{2+}$  are different in line height and spacing. In addition to these allowed  $\Delta M_S = \pm 1$ ,  $\Delta M_I = 0$  transitions, lines corresponding to forbidden  $\Delta M_S = \pm 1$ ,  $\Delta M_I = \pm 1$  transitions appear as five doublets between the six hyperfine components of the allowed transitions. This is typical of the  $\text{Mn(II)}$  ion, which is under axial distortion. These manganese complexes are mononuclear, since there is no superimposed broad singlet from interacting  $\text{Mn(II)}$  ions [26].

Both EPR spectra can be simulated by the superposition of two signals, which allows the determination of the anisotropic *g* values, the anisotropic hyperfine constants and the zero-field splitting parameters (Table 3). The parameters of both components that may correspond to two different complexes between the layers are similar to each other. This statement is in good agreement with the quantitative analysis of the intercalant, since it shows that besides the major complexes with 2:1 amino acid: $\text{Mn}^{2+}$  ratio, complexes with 3:1 ratio were also formed, albeit in small quantities (the amino acid/metal ion ratios are higher than 2 for both composites).

The observed  $g_{av}$  values are very close to the free electron *g* value, suggestive of the absence of spin-orbit coupling in the ground state. These data are not a good source of information about electronic structures of the investigated complexes.

The  $^{55}\text{Mn}$   $A_{av}$  values suggest that the  $\text{Mn}^{2+}$  ions are in octahedral coordination environment [27].

The zero-field splitting is very sensitive to the environment of the  $\text{Mn(II)}$  ion. The magnitude of *D* determined for octahedral  $[\text{MnL}_6]^{n+}$  complexes ranges from 0.00087 to 0.1750  $\text{cm}^{-1}$ . For mono- or bidentate ligands, the *D* values are smaller, and fall in the range of 0.00087 and 0.0673  $\text{cm}^{-1}$ , while for tri-, tetra- or pentadentate ligands the values are between 0.0420 and 0.1750  $\text{cm}^{-1}$  [28].

Putting together these pieces of information, we propose, that two different, isolated, octahedral  $\text{Mn(II)}$  complexes coordinated with mono and/or bidentate ligands are located between the layers for both intercalated samples studied, indicated as comp. 1 and comp. 2 in Table 3.

Generally speaking, XAS measurements (Fig. 10 and Table 4) also indicated octahedral coordination environment.

Moreover, it was also revealed that the thiolate sulfur in the cysteine ligand was a coordination site. The amino nitrogens in all three composites and the phenolate oxygen in  $\text{Mn(II)-tyrosinate-Ca}_2\text{Al-LDH}$  may also be coordinated. The carboxylate oxygens are probably used in the intercalation process; nevertheless, they might take part in coordinating the  $\text{Mn}^{2+}$  ion as well. Let us note that XAS cannot differentiate between oxygen and nitrogen. Since the analytical data in Table 1 indicated the amino acid to  $\text{Mn}^{2+}$  ratios were close to 2, it is assumed that the amino acids acted mostly as bidentate ligands, and to fill the still available two positions, we have to assume the participation of two water molecules.

Far IR spectroscopy can give direct information on metal-functional group interactions, and thus it can be useful in verifying and/or complementing those obtained from EPR and XAS measurements.

In Fig. 11, the decomposed far IR spectra of the host as well as the intercalated materials are displayed.

Beside the intense bands of the host LDH, in the spectra of  $\text{Mn(II)-cysteinate-Ca}_2\text{Al-LDH}$ , and  $\text{Mn(II)-tyrosinate-Ca}_2\text{Al-LDH}$ , a new band is seen at the low frequency, at 330  $\text{cm}^{-1}$ . On the basis

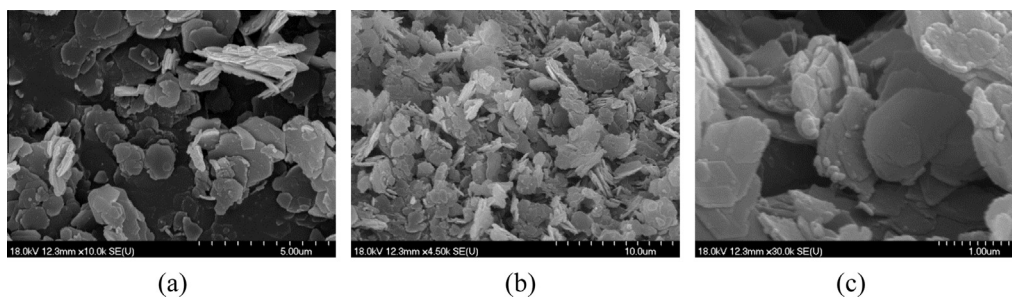


Fig. 7. The SEM images of (a) Mn(II)-cysteinate- $\text{Ca}_2\text{Al-LDH}$ , (b)  $\text{Ca}_2\text{Al-Mn(II)-histidinate-LDH}$  and (c) Mn(II)-tyrosinate- $\text{Ca}_2\text{Al-LDH}$  at various magnifications.

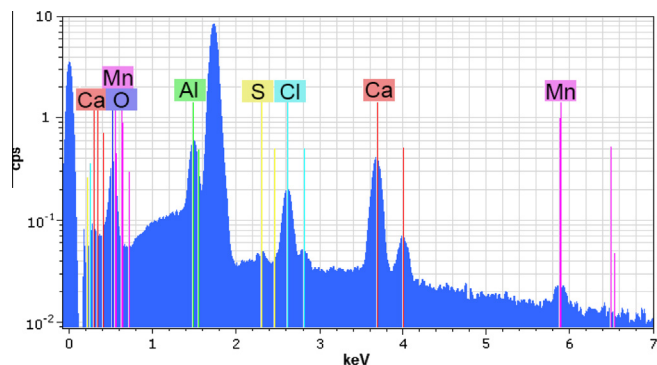


Fig. 8. EDX spectrum of the Mn(II)-cysteinate- $\text{Ca}_2\text{Al-LDH}$  sample.

of our previous study [29] concerning (among others) Mn(II) complexes with ligand having only one type of group capable of coordination, this band is assigned to  $\text{Mn(II)-O}_{\text{carboxylate}}$  vibration. This band was not found for the  $\text{Ca}_2\text{Al-Mn(II)-histidinate-LDH}$  substance indicating that the carboxylate group was not coordinated to Mn(II); however, the new band at  $293\text{ cm}^{-1}$  can be attributed

to  $\text{Mn(II)-N}_{\text{imidazole}}$  interaction [29], which is known to be the typical metal- $\text{N}_{\text{imidazole}}$  coordination mode. Sign for the coordination of the amino group is masked by the LDH vibrations and the bands near and above  $400\text{ cm}^{-1}$  signal the coordination of water molecules [29].

To sum up, in each case octahedral coordination is proposed with the coordination of two water molecules and two amino acid anions acting as bidentate ligands. In the  $\text{Ca}_2\text{Al-Mn(II)-histidinate-LDH}$  sample (prepared by Method 1), the carboxylate groups interact with the layers of the LDH. The imidazole nitrogen was identified as the coordinating site, and the other possibility remained the amino nitrogen. In the Mn(II)-tyrosinate- $\text{Ca}_2\text{Al-LDH}$  sample, the carboxylate group and the amino nitrogen or the phenolate oxygen take part in the coordination. In the Mn(II)-cysteinate- $\text{Ca}_2\text{Al-LDH}$  material, the coordination sites are the carboxylate groups and the S atom of the ligand. These latter two substances were intercalated under basic conditions to facilitate deprotonation; thus, they could be immobilized between the layers via electrostatic interactions. For the Mn(II)-cysteinate- $\text{Ca}_2\text{Al-LDH}$  and the  $\text{Ca}_2\text{Al-Mn(II)-histidinate-LDH}$  samples, analytical data indicated that there may be complexes among the layers with three coordinated amino acid anions although in small quantities. The possible arrangements of the

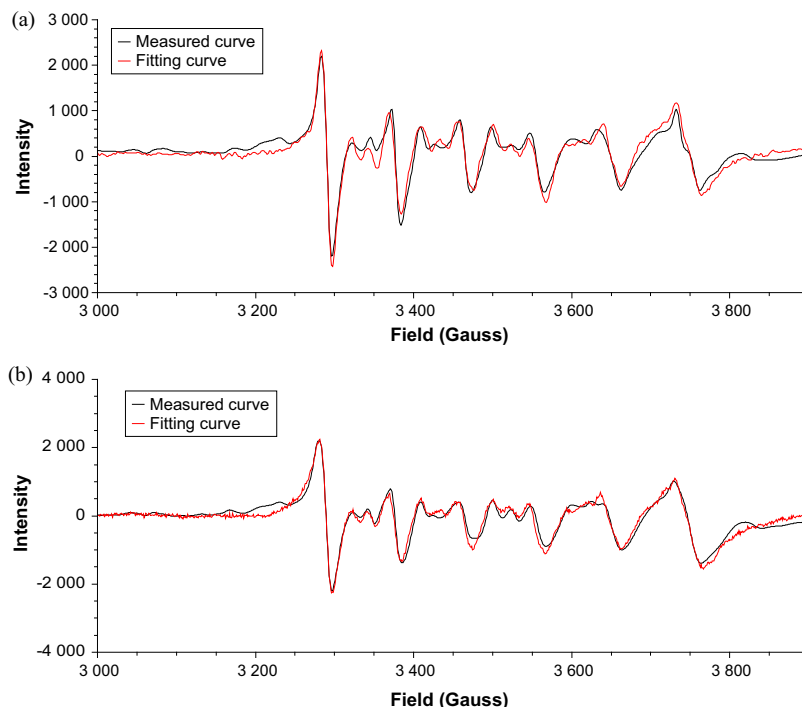
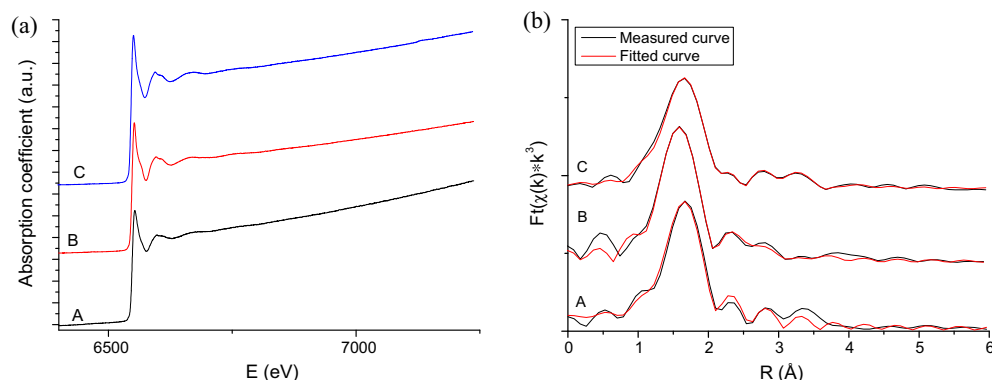


Fig. 9. The measured and fitted EPR spectra of (a)  $\text{Ca}_2\text{Al-Mn(II)-histidinate-LDH}$  and (b) Mn(II)-cysteinate- $\text{Ca}_2\text{Al-LDH}$ .

**Table 3**  
EPR parameters of the two selected intercalated samples.

Ca <sub>2</sub> Al-LDH sample	$g_x$	$g_y$	$g_z$	$g_{av}$	$A_x$ (cm <sup>-1</sup> )	$A_y$ (cm <sup>-1</sup> )	$A_z$ (cm <sup>-1</sup> )	$A_{av}$ (cm <sup>-1</sup> )	$D$ (cm <sup>-1</sup> )	$E$ (cm <sup>-1</sup> )
Mn(II)-His (comp. 1)	1.9840	2.0091	2.0182	2.0038	0.0084	0.0098	0.0092	0.0091	0.0261	0.0015
Mn(II)-His (comp. 2)	1.9852	1.9908	2.0360	2.0040	0.0082	0.0090	0.0061	0.0077	0.0185	0.0030
Mn(II)-Cys (comp. 1)	1.9803	2.0072	2.0188	2.0021	0.0083	0.0096	0.0091	0.0090	0.0267	0.0015
Mn(II)-Cys (comp. 2)	1.9825	1.9849	2.0357	2.0010	0.0084	0.0086	0.0062	0.0077	0.0195	0.0028



**Fig. 10.** X-ray absorption spectra of A: Mn(II)-tyrosinate–Ca<sub>2</sub>Al-LDH, B: Ca<sub>2</sub>Al–Mn(II)-histidinate–LDH and (C) Mn(II)-cysteinate–Ca<sub>2</sub>Al-LDH; (a) the measured and (b) the Fourier-transformed (without phase correction) spectra.

**Table 4**  
Parameters calculated from the fitted EXAFS spectra ( $N$ : coordination number,  $R$ : bond length,  $\sigma^2$  Debye–Waller factor, F-factor: goodness of fit).

Ca <sub>2</sub> Al-LDH sample	Mn(II)–X	$N$	$R$ (Å)	$\sigma^2$ (Å <sup>2</sup> )	F-factor
Mn(II)-tyrosinate	N/O	6	2.18	0.0045	0.197
Mn(II)-cysteinate	N/O	4	2.16	0.0075	0.084
	S	2	2.57	0.0173	
Mn(II)-histidinate	N/O	6	2.19	0.01139	0.122

complexes between the layers were modeled mainly for visualization. For this, the 0.234 nm was chosen as the thickness of the hydroxide layer, which was derived from single crystal XRD [30], and the basal spacings ( $d$ ) obtained from powder X-ray diffractograms. Models for the complexes were constructed on the basis

of EPR, XAS and far IR measurements applying the EXAFS data for setting the bond distances. During building the model, it was revealed that the phenolate oxygen in the tyrosinate and the carboxylate oxygen cannot coordinate at the same time due to steric reasons; therefore, the carboxylate group and the amino nitrogen are proposed as coordination sites. The models and the relevant size data are shown in Fig. 12 and in Table 5, respectively.

### 3.4. Catalytic properties in oxidative transformations

Cyclohexene and two oxidants [peracetic acid and (diacetoxy) iodobenzene] were chosen as the probe molecules for studying the catalytic properties of the intercalated samples. The oxidation reaction of cyclohexene can lead to a number of products as shown in Scheme 1.

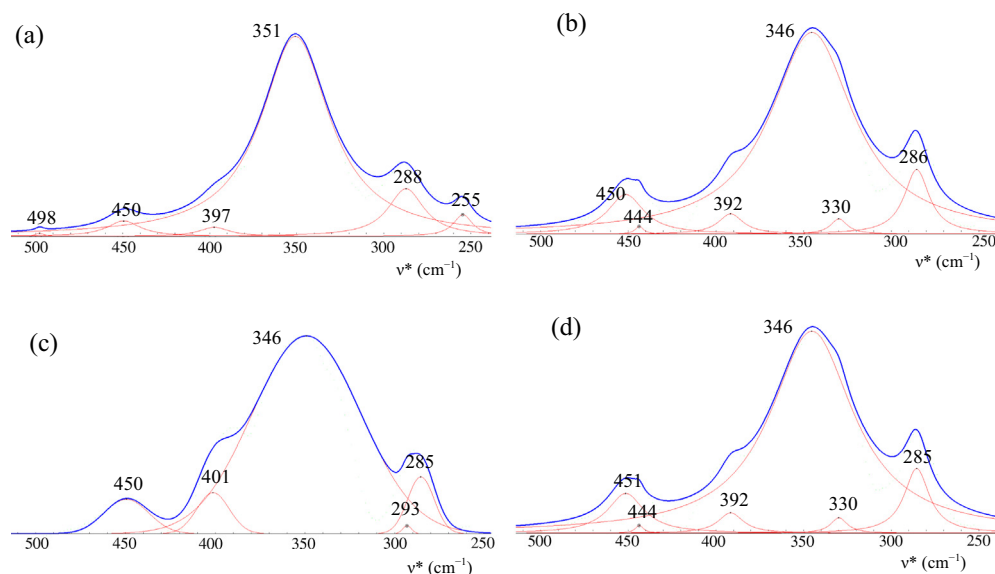


**Fig. 11.** The decomposed far IR spectra of (a) Ca<sub>2</sub>Al-LDH, (b) Mn(II)-cysteinate–Ca<sub>2</sub>Al-LDH, (c) Ca<sub>2</sub>Al–Mn(II)-histidinate–LDH and (d) Mn(II)-tyrosinate–Ca<sub>2</sub>Al-LDH.

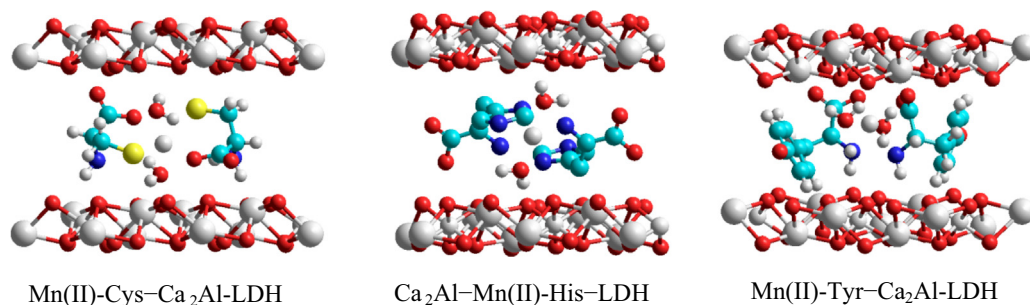
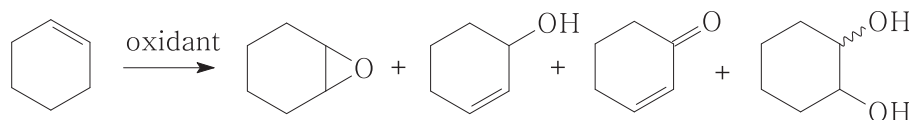


Fig. 12. The proposed steric arrangement of the intercalated complexes between the layers of  $\text{Ca}_2\text{Al-LDH}$ , based on XRD and XAS measurements.

Table 5

Dimensions of the intercalated LDHs and the complexes (thickness of one layer is 0.234 nm).

Substances	Basal spacing ( $d$ ) (nm)	Interlayer spacing (nm)	Dimension data of the complexes (nm)
Mn(II)-Cys- $\text{Ca}_2\text{Al-LDH}$	0.921	0.687	$0.447 \times 0.447 \times 0.959$
$\text{Ca}_2\text{Al-Mn(II)-His-LDH}$	0.929	0.695	$0.697 \times 0.496 \times 1.030$
Mn(II)-Tyr- $\text{Ca}_2\text{Al-LDH}$	0.859	0.625	$0.660 \times 0.475 \times 1.238$



Scheme 1. The oxidative transformations of cyclohexene.

Table 6

The TOF/conversion and selectivity results of the oxidation of cyclohexene after 3 h (catalyst: 25 mg, acetone: 10  $\text{cm}^3$ , cyclohexene: 5 mmol, peracetic acid: 2.5 mmol, temperature: 298 K).

Catalyst	TOF (1/h)/conversion (%)	Epoxide (%)	2-Chex-1-ol (%)	2-Chex-1-one (%)	<i>trans</i> -Diol (%)
–	nr/21	64	4	2	30
$\text{Ca}_2\text{Al-LDH}$	nr/18	63	4	5	28
Mn(II)-Tyr- $\text{Ca}_2\text{Al-LDH}$	31/33	79	0	0	21
Mn(II)-Cys- $\text{Ca}_2\text{Al-LDH}$	38.5/40	100	0	0	0
$\text{Ca}_2\text{Al-Mn(II)-His-LDH}$	50/53	100	0	0	0

The major products are expected to be the epoxide (a result of mild oxidation) and alcohols if the oxidant is stronger; thus, beside activity, the possible selectivity changes may be studied as well.

Let us consider the peracetic acid oxidant first. The manganese complexes would be active in the decomposition of peroxides as well as for the peracetic acid. Fortunately, in acetone, the peroxide is protected against decomposition [31]; therefore, acetone was the chosen solvent. This protective property was checked; our composite materials did not promote the decomposition of peracetic acid. Peracetic acid alone (without any catalyst) is a known epoxidation agent. Indeed, epoxidation did occur in our hands as well. In the experiment using the pristine LDH, the conversion and the selectivity values were very close to that when peracetic acid was used in the absence of the Mn(II) complex-intercalated LDHs. The TOF/conversion values as well as selectivity data are seen in Table 6.

In the presence of the intercalated manganese complexes, the transformation of cyclohexene accelerated appreciably, and the conversions did not vary dramatically. More importantly, the epoxide selectivity also increased considerably, relative to the uncatalyzed transformation, for Mn(II)-tyrosinate- $\text{Ca}_2\text{Al-LDH}$ , and it became fully selective over the other two catalysts. The catalysts did not undergo any color change during the reaction, and there

was no leaching of the ligands or the complex either, as the analysis of the product mixture (gas chromatography and ICP-OES measurements) as well as repeated (recycling) reactions attested. The catalysts could be reactivated by simple rinsing with acetone, and they could work again with practically no changes in activities (Table 7).

Although the identity of the ligands modified the selectivity somewhat, in our view, the major role of the ligands is influencing the accessibility of the central ion. In the presence of the intercalated complex, direct coordination of the peracetic acid to the central ion may occur, replacing water molecule in the coordination

Table 7

Conversions in three rounds of recycling in the oxidation of cyclohexene after 3 h (catalyst: 25 mg, acetone: 10  $\text{cm}^3$ , cyclohexene: 5 mmol, peracetic acid: 2.5 mmol, temperature: 298 K, reactivation: rinsing with acetone).

Catalyst	Conversion (%)		
	1st recycle	2nd recycle	3rd recycle
Mn(II)-tyrosinate- $\text{Ca}_2\text{Al-LDH}$	35	33	33
Mn(II)-cysteinate- $\text{Ca}_2\text{Al-LDH}$	40	42	43
$\text{Ca}_2\text{Al-Mn(II)-histidinate-LDH}$	49	47	45

**Table 8**

The TOF/conversion and selectivity results of the oxidation of cyclohexene after 3 h (catalyst: 25 mg, aqueous acetone (5/95% by volume); 10 cm<sup>3</sup>, cyclohexene: 5 mmol, (diacetoxyiodo)benzene acid: 2.5 mmol, temperature: 298 K).

Catalyst	TOF (1/h)/conversion (%)	Epoxide (%)	2-Chex-1-ol (%)	2-Chex-1-one (%)	cis Diol (%)
–	Nr/19	49	28	17	6
Mn(II)-Tyr–Ca <sub>2</sub> Al-LDH	28/30	12	0	0	88
Mn(II)-Cys–Ca <sub>2</sub> Al-LDH	35.6/37	5	0	0	95
Ca <sub>2</sub> Al–Mn(II)-His–LDH	47.2/50	7	0	0	93

sphere, and oxygen transfer to the double bond of the possibly uncoordinated cyclohexene takes place at this stage. This should be the reason of the outstanding epoxide selectivity.

This mechanistic suggestion resembles that of Jacobsen–Katsuki epoxidation [32,33], except decomposition of the peracetic acid to Mn=O-like species does not take place, and oxygen transfer occurs from the coordinated peracetic acid. If both reactants were coordinated, there would be plenty of time for further reactions. If cyclohexene was coordinated alone, the situation would not be much different from the stoichiometric reaction.

Cyclohexene was oxidized, under similar conditions, with (diacetoxyiodo)benzene in aqueous acetone, too. The composition of the reacting mixture was the same except aqueous acetone (5/95% by volume) was the solvent. Water was needed for hydrolysis, and thus the activation of (diacetoxyiodo)benzene by the following transformation [34]:



The TOF/conversion and selectivity values obtained with the *in situ* generated PhI(OH)<sub>2</sub> are displayed in Table 8.

Data revealed that the *in situ* formed PhI(OH)<sub>2</sub>, in the presence of added intercalated complexes produced almost exclusively the diol even though epoxide was formed in appreciable quantities without them. The added composites acted as catalysts, and largely retained their activities (Table 9) even in the third recycling experiments, and again, they were only rinsed with the solvent after each run as the regeneration step. During recycling, only the diol was formed in the presence of each catalyst. Diol was a primary product over the fresh as well as the recycled catalysts, since the *cis* isomer was only observed. If it had been originated from the ring opening of the epoxide, the *trans* isomer would have been formed.

The catalysts were also tested in the oxidative transformations of allylic alcohol with peracetic acid as the oxidant. Here, epoxidation only occurred resulting in glycidol formation exclusively (Scheme 2).

The epoxidation of allylic alcohol was significantly slower than that of cyclohexene; the optimum conditions were 60 mg of catalyst, 6 h of reaction time and 333 K of reaction temperature, keeping the composition of the reacting mixture the same as with cyclohexene. Again, epoxidation did occur in the homogeneous reaction; however, the reaction rate/% conversion substantially increased in the presence of the intercalated materials (Table 10).

**Table 9**

Conversions in three rounds of recycling in the oxidation of cyclohexene after 3 h (catalyst: 25 mg, aqueous acetone (5/95% by volume); 10 cm<sup>3</sup>, cyclohexene: 5 mmol, (diacetoxyiodo)benzene: 2.5 mmol, temperature: 298 K, reactivation: rinsing with acetone).

Catalyst	Conversion (%)		
	1st recycle	2nd recycle	3rd recycle
Mn(II)-tyrosinate–Ca <sub>2</sub> Al-LDH	31	27	25
Mn(II)-cysteinate–Ca <sub>2</sub> Al-LDH	29	28	28
Ca <sub>2</sub> Al–Mn(II)-histidinate–LDH	48	45	47

**Scheme 2.** Glycidol formation in the epoxidation of allylic alcohol.**Table 10**

The TOF/conversion and selectivity results of the oxidation of allylic alcohol after 6 h (catalyst: 60 mg, acetone: 10 cm<sup>3</sup>, cyclohexene: 5 mmol, peracetic acid: 2.5 mmol, temperature: 333 K).

Catalyst	TOF (1/h)/conversion (%)	Glycidol (%)
–	nr/16	100
Ca <sub>2</sub> Al-LDH	nr/16	100
Mn(II)-tyrosinate–Ca <sub>2</sub> Al-LDH	18.8/48	100
Mn(II)-cysteinate–Ca <sub>2</sub> Al-LDH	15.2/38	100
Ca <sub>2</sub> Al–Mn(II)-histidinate–LDH	20/51	100

In the absence as well as in the presence of the composites, epoxidation only took place.

#### 4. Conclusions

Three composite materials having Mn(II)-amino acid complexes among the layers of CaAl-LDH were successfully synthesized *via* either sequential intercalation (introducing the ligands first, then constructing the complex – Ca<sub>2</sub>Al–Mn(II)-histidinate–LDH) or direct intercalation of the preformed complex (Mn(II)-cysteinate–Ca<sub>2</sub>Al-LDH and Mn(II)-tyrosinate–Ca<sub>2</sub>Al-LDH). The aim of having the complexes exclusively among the layers of the LDH was achieved, which was verified by using a range of instrumental methods (XRD, SEM measurements, diffuse reflectance, ATR- and PA-IR spectroscopies).

The intercalant was also characterized by relevant, mostly instrumental methods (classical chemical and energy dispersive X-ray analysis, EPR, X-ray absorption and far IR spectroscopies) revealing a coordination number of six, and the imidazole nitrogen, the carboxylate group and the thiolate sulfur as sure coordination sites.

The intercalated substances were efficient, recyclable catalysts tested in the oxidation reactions of cyclohexene with two different oxidants giving two different products with very high selectivities (peracetic acid: epoxide, *in situ* formed iodosylbenzene: *cis* diol). However, allylic alcohol only gave the epoxide with peracetic acid.

#### Acknowledgment

This work was supported by the National Science Fund of Hungary through Grant OTKA NKFI 106234. The financial help is highly appreciated.

#### Appendix A. Supplementary material

Supplementary data associated with this article can be found, in the online version, at <http://dx.doi.org/10.1016/j.jcat.2015.12.023>.

## References

- [1] A. de Roy, C. Forano, J.P. Besse, in: V. Rives (Ed.), *Layered Double Hydroxides*, Ch. 1: Layered Double Hydroxides: Synthesis and Post-synthesis Modification, Nova Science Publishers, Inc., 2001, pp. 1–39.
- [2] J. He, M. Wei, B. Li, Y. Kang, D.G. Evans, X. Duan, Preparation of layered double hydroxides, *Struct. Bond.* 119 (2005) 89–119.
- [3] V. Tóth, M. Sipiczki, A. Pallagi, Á. Kukovecz, Z. Kónya, P. Sipos, I. Pálincó, Synthesis and properties of CaAl-layered double hydroxide (CaAl-LDH) of the hydrocalumite type, *Chem. Pap.* 68 (2014) 633–637.
- [4] Zs. Ferencz, Á. Kukovecz, Z. Kónya, P. Sipos, I. Pálincó, Optimisation of the synthesis parameters of mechanochemically prepared CaAl-layered double hydroxide, *Appl. Clay Sci.* 112–113 (2015) 94–99.
- [5] C. Forano, T. Hibino, F. Leroux, C. Taviot-Guého, in: F. Bergaya, B.K.G. Theng, G. Lagaly (Eds.), *Handbook of Clay Science, Developments in Clay Science*, Ch. 13.1: Layered Double Hydroxides, vol. 1, Elsevier LTD, 2006, pp. 1021–1095.
- [6] I. Pálincó, in: H.S. Nalwa (Ed.), *Encyclopedia of Nanoscience and Nanotechnology, Nanostructures in Confined Environments*, vol. 19, American Scientific Publishers, 2011, pp. 183–198.
- [7] A.I. Khan, D. O'Hare, Intercalation chemistry of layered double hydroxides: recent developments and applications, *J. Mater. Chem.* 12 (2002) 3191–31918.
- [8] G. Choi, J.-H. Yang, G.-Y. Park, A. Vinu, A. Elzatahy, C.H. Yo, J.-H. Choy, Intercalative ion-exchange route to amino acid layered double hydroxide nanohybrids and their sorption properties, *Eur. J. Inorg. Chem.* (2015) 925–930.
- [9] Zs. Ferencz, M. Ádok-Sipiczki, I. Hannus, P. Sipos, I. Pálincó, Structural features of intercalated CaFe-layered double hydroxides studied by X-ray diffractometry, infrared spectroscopy and computations, *J. Mol. Struct.* 1090 (2015) 14–18.
- [10] B.M. Choudary, B. Kavita, N.S. Chowdary, B. Sreedhar, M.L. Kantam, Layered double hydroxides containing chiral organic guests: Synthesis, characterization and application for asymmetric C–C bond-forming reactions, *Catal. Lett.* 78 (2002) 373–377.
- [11] S. Miyata, Physico-chemical properties of synthetic hydrotalcites in relation to composition, *Clays Clay Miner.* 28 (1980) 50–56.
- [12] M. Sipiczki, E. Kuzmann, I. Pálincó, Z. Homonnay, P. Sipos, Á. Kukovecz, Z. Kónya, Mössbauer and XRD study of intercalated CaFe-layered double hydroxides, *Hyperfine Interact.* 226 (2014) 171–179.
- [13] Zs. Ferencz, M. Szabados, G. Varga, Z. Csenedes, Á. Kukovecz, Z. Kónya, S. Carlson, P. Sipos, I. Pálincó, Mechanochemical synthesis and intercalation of Ca(II)Fe(III)-layered double hydroxides, *J. Solid State Chem.* 233 (2016) 236.
- [14] M. Milanese, E. Conteroso, D. Viterbo, L. Perioli, G. Croce, New efficient intercalation of bioactive molecules into layered double hydroxide materials by solid-state exchange: an in situ XRPD study, *Crystr Growth Des.* 10 (2010) 4710–4712.
- [15] V. Rives, M.A. Ulibarri, Layered double hydroxides (LDH) intercalated with metal coordination compounds and oxometalates, *Coord. Chem. Rev.* 181 (1999) 61–120.
- [16] E. Coronado, J.R. Galán-Mascarós, C. Martí-Gastaldo, A. Ribera, Insertion of magnetic bimetallic oxalate complexes into layered double hydroxides, *Chem. Mater.* 18 (2006) 6112–6114.
- [17] S. Bhattacharjee, J.A. Anderson, Synthesis and characterization of novel chiral sulfonate-salen-manganese(III) complex in a zinc-aluminium LDH host, *Chem. Commun.* (2004) 554–555.
- [18] S. Bhattacharjee, J.A. Anderson, Epoxidation by layered double hydroxide-hosted catalysts. Catalyst synthesis and use in the epoxidation of R-(+)-limonene and (–)- $\alpha$ -pinene using molecular oxygen, *Catal. Lett.* 95 (2004) 119–125.
- [19] S. Bhattacharjee, T.J. Dines, J.A. Anderson, Synthesis and application of layered double hydroxide-hosted catalysts for stereoselective epoxidation using molecular oxygen or air, *J. Catal.* 225 (2004) 398–407.
- [20] S. Bhattacharjee, J.A. Anderson, Novel chiral sulphonato-salen-manganese(III)-pillared hydrotalcite catalysts for the asymmetric epoxidation of styrenes and cyclic alkenes, *Adv. Synth. Catal.* 348 (2006) 151–158.
- [21] S. Bhattacharjee, T.J. Dines, J.A. Anderson, Comparison of Co with Mn and Fe in LDH-hosted sulfonate-salen catalysts for olefin epoxidation, *J. Phys. Chem. C* 112 (2008) 14124–14130.
- [22] L. Dai, J. Zhang, X. Wang, Y. Chen, The direct assembly of Mg–Al LDH nanosheets and Mn(II)–salen complex into sandwich-structured materials and their enhanced catalytic properties, *RSC Adv.* 3 (2013) 19885–19888.
- [23] Y. Liu, Z. An, L. Zhao, H. Liu, J. He, Enhanced catalytic efficiency in the epoxidation of alkenes for manganese complex encapsulated in the hydrophobic interlayer region of layered double hydroxides, *Ind. Eng. Chem. Res.* 52 (2013) 17821–17828.
- [24] G.N. George, I.F. Pickering, EXAFSPAK – A suite of computer programs for analysis of X-ray absorption spectra, Stanford Synchrotron Radiation Laboratory, Stanford, CA, 1995. <<http://www-ssrl.slac.stanford.edu/exafspak.html>> (accessed September, 2015).
- [25] A. Rockenbauer, L. Korecz, Automatic computer simulations of ESR spectra, *Appl. Magn. Res.* 10 (1996) 29–43.
- [26] Z. Luan, J. Xu, L. Kevan, Manganese–bipyridine complex incorporated into mesoporous MCM-41 molecular sieves, *Chem. Mater.* 10 (1998) 3699–3706.
- [27] P.F. Rapheal, E. Manoj, M.R. Prathapachandra Kurup, Syntheses and EPR spectral studies of manganese(II) complexes derived from pyridine-2-carbaldehyde based N(4)-substituted thiosemicarbazones: crystal structure of one complex, *Polyhedron* 26 (2007) 5088–5094.
- [28] C. Duboc, M.-N. Collomb, F. Neese, Understanding the zero-field splitting of mononuclear manganese(II) complexes from combined EPR spectroscopy and quantum chemistry, *Appl. Magn. Reson.* 37 (2010) 229–245.
- [29] G. Varga, Z. Csenedes, G. Peintler, O. Berkesi, P. Sipos, I. Pálincó, Using far IR spectra for the unambiguous identification of metal ion–ligand coordination sites in purpose-built complexes, *Spectrochim. Acta, A* 122 (2014) 257–259.
- [30] M. Sacerdoti, E. Passaglia, In *Neues Jahrbuch für Mineralogie, Monatshefte* 1988, Hydrocalumite from Latium, Italy: Its Crystal Structure and Relationship with Related Phases, pp. 462–475.
- [31] D.E. de Vos, B.F. Sels, P.A. Jacobs, Heterogeneous enzyme mimics based on zeolites and layered hydroxides, *Cattech* 6 (2002) 14–29.
- [32] W. Zhang, J.L. Loebach, S.R. Wilson, E.N. Jacobsen, Enantioselective epoxidation of unfunctionalized olefins catalyzed by salen manganese complexes, *J. Am. Chem. Soc.* 112 (1990) 2801–2803.
- [33] R. Irie, K. Noda, Y. Ito, N. Matsumoto, T. Katsuki, Catalytic asymmetric epoxidation of unfunctionalized olefins, *Tetrahedron Lett.* 31 (1990) 7345–7348.
- [34] J.-H. In, S.-E. Park, R. Song, W. Nam, Iodobenzene diacetate as an efficient terminal oxidant in iron(III) porphyrin complex-catalyzed oxygenation reactions, *Inorg. Chim. Acta* 343 (2003) 373–376.